Direct Model Predictive Current Control of Quasi-Z-Source Inverters

Ayman Ayad, Petros Karamanakos, Ralph Kennel
Institute of Electrical Drive Systems and Power Electronics
Technical University of Munich, Munich, Germany
Email: ayman.f.ayad@ieee.org, p.karamanakos@ieee.org, kennel@ieee.org

***Abstract*—This paper introduces a direct model predictive control (MPC) strategy to control both sides of a quasi-Z-source inverter (qZSI) based on the inductor and the output currents. To improve the performance of the controlled system, a long prediction horizon is implemented. However, the underlying optimization problem may become computationally intractable because of the increased computational power demands. To overcome this and to solve the problem in real time in a computationally efficient manner, a branch-and-bound strategy is used along with a move blocking scheme. Simulation results highlight the effectiveness of the presented control strategy.**

I. Introduction

Z-source inverter (ZSI) was proposed in 2003 as an efficient alternative to the traditional two-stage buck-boost inverter. The ZSI fulfills the buck-boost function in a single-stage inverter [1], resulting in an enhanced efficiency and reduced cost compared to the traditional two-stage inverter [2]. The quasi-Z-source inverter (qZSI) was presented as an improved version of the classical ZSI [3]. It has many advantages such as continuous input current and joint earthing of the dc-source and the dc-link bus. Moreover, the voltage of one of the quasi-Z-source network capacitors is significantly reduced resulting in a smaller passive components size [4], [5].

Using traditional linear control techniques to control the qZSI appears to be a challenging task. The main reason is that the capacitor voltages (the dc-link voltage) and the inductor currents on the dc-side of the converter have to be controlled at the same time with the controlled variables on the ac-side. Hence, the design of a linear controller becomes cumbersome, since many cascaded loops are required [4], [6], [7]. As an alternative, nonlinear control algorithms such as sliding mode control [8] and neural network control [9] have been applied to ZSI/qZSI. In comparison with the traditional proportional-integral (PI) based control, these algorithms exhibit fast dynamic behaviors, at the expense though of a further increase in the design complexity.

Over the last decade, model predictive control (MPC) [10] has been established as an attractive control algorithm for power electronics applications [11]. Particularly, the so called *direct* MPC—also referred to as finite control set (FCS) MPC—has been extensively used, thanks to its design simplicity; the switches of the converter are directly manipulated without requiring a modulator [11]–[13]. Moreover, MPC, in general, and direct MPC, in particular, have been proved to be particularly effective when multiple-input multiple-output (MIMO) systems are concerned with nonlinear, complex dynamics. The reason is that all the control objectives can be tackled in one stage since they are incorporated in one performance criterion, i.e. the cost function.

Considering the complexity of the qZSI, in this paper a direct MPC algorithm—implemented as a current controller—is adopted to handle the multiple control objectives. Up-to-date, only a few research works have been focused on MPC for ZSI/qZSI, e.g. [14]–[16]. It is noteworthy that the aforementioned works use a one-step horizon MPC. However, a single-step horizon MPC is not sufficient to achieve a good system performance, especially when applied to complex systems [17] such as the qZSI. Therefore, in this work, a long-horizon MPC is implemented to achieve an improved performance. Nevertheless, since the computational complexity grows exponentially with the length of the prediction horizon, strategies need to be employed that balance the trade-off between the length of the prediction horizon and the number of computations required. To keep the computational complexity modest, a branch-and-bound technique [18] is employed combined with a move blocking scheme [19] that yields a nontrivial prediction horizon. Simulation results are presented to verify the performance of the proposed approach.

II. Physical Model of Quasi-Z-Source Inverter

Fig. 1 shows the configuration of the qZSI consisting of a quasi-Z-source network, a three-phase two-level inverter, and an RL load. With the inductors, L_1, L_2, and the capacitors, C_1, C_2, the qZSI manages to deliver a dc voltage v_{dc} that can be either equal to, or higher than the input voltage v_{in}. Consequently, it has two modes of operation, i.e. a buck and boost mode. During the buck mode, the converter operates as the traditional two-level inverter. In boost mode, the qZSI introduces two operation states, namely the non-shoot-through and the shoot-through states, see Fig. 2 [16].

The system states include the output current[1], the inductor currents, and the capacitor voltages. Thus, the state vector is $\boldsymbol{x} = [i_{o,\alpha}\ i_{o,\beta}\ i_{L_1}\ i_{L_2}\ v_{C_1}\ v_{C_2}]^T \in \mathbb{R}^6$. The three-phase

[1]To ease the computations it is common practice to express a variable in the stationary orthogonal system $(\alpha\beta)$ instead of the three-phase system (abc), i.e. $\boldsymbol{\xi}_{\alpha\beta} = \boldsymbol{K}\boldsymbol{\xi}_{abc}$, where $\boldsymbol{K}$ is the transformation matrix of appropriate dimensions. Note, though, that, the subscript for vectors in the $\alpha\beta$ plane is dropped within the text to simplify the notation. Vectors in the abc plane are denoted with the corresponding subscript.

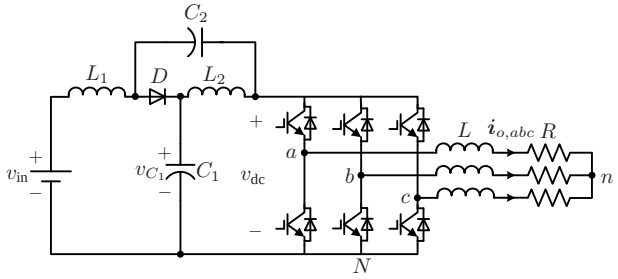

Fig. 1: Topology of the quasi-Z-Source Inverter (qZSI).

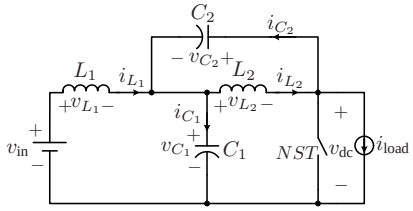

(a) Non-shoot-through state.

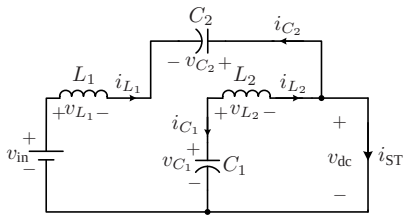

(b) Shoot-through state.

Fig. 2: Operation states of the qZSI during the boost mode.

switching positions $\boldsymbol{u}_{abc} \in \mathcal{U}^3$ are considered as the input to the system, with $\boldsymbol{u}_{abc} = [u_a \; u_b \; u_c]^T$ and $\mathcal{U} = \{0, 1\}$. In addition, the output and the inductor currents are the output variables, i.e. $\boldsymbol{y} = [i_{o,\alpha} \; i_{o,\beta} \; i_{L_1}]^T \in \mathbb{R}^3$. Finally, the input voltage is considered as a disturbance to the system, i.e. $\boldsymbol{w} = v_{\text{in}} \in \mathbb{R}$.

First the model of the converter is derived when the non-shoot-through state is considered, and in a subsequent step, the qZSI model with the shoot-through state is examined.

A. Non-Shoot-Through State

At non-shoot-through state, as can be seen in Fig. 2(a), the diode is conducting, thus the input voltage source and the inductors deliver energy to the capacitors and the load. Accordingly, the system model is given by

$$\frac{\mathrm{d}\boldsymbol{x}(t)}{\mathrm{d}t} = \boldsymbol{F}_1\boldsymbol{x}(t) + \boldsymbol{G}_1\boldsymbol{u}_{abc}(t) + \boldsymbol{H}_1\boldsymbol{w}(t) \tag{1a}$$

$$\boldsymbol{y}(t) = \boldsymbol{E}\boldsymbol{x}(t)\,, \tag{1b}$$

where

$$\boldsymbol{F}_1 = \begin{bmatrix} -\frac{R}{L} & 0 & 0 & 0 & 0 & 0 \\ 0 & -\frac{R}{L} & 0 & 0 & 0 & 0 \\ 0 & 0 & 0 & 0 & -\frac{1}{L_1} & 0 \\ 0 & 0 & 0 & 0 & 0 & -\frac{1}{L_2} \\ -\frac{\boldsymbol{u}_{abc}^T\boldsymbol{K}_{(:,1)}^{-1}}{C_1} & -\frac{\boldsymbol{u}_{abc}^T\boldsymbol{K}_{(:,2)}^{-1}}{C_1} & \frac{1}{C_1} & 0 & 0 & 0 \\ -\frac{\boldsymbol{u}_{abc}^T\boldsymbol{K}_{(:,1)}^{-1}}{C_2} & -\frac{\boldsymbol{u}_{abc}^T\boldsymbol{K}_{(:,2)}^{-1}}{C_2} & 0 & \frac{1}{C_2} & 0 & 0 \end{bmatrix},$$

$$\boldsymbol{G}_1 = \hat{v}_{\text{dc}} \begin{bmatrix} \frac{1}{L} & 0 \\ 0 & \frac{1}{L} \\ 0 & 0 \\ 0 & 0 \\ 0 & 0 \\ 0 & 0 \end{bmatrix} \boldsymbol{K}, \qquad \boldsymbol{H}_1 = \begin{bmatrix} 0 \\ 0 \\ \frac{1}{L_1} \\ 0 \\ 0 \\ 0 \end{bmatrix},$$

$$\boldsymbol{E} = \begin{bmatrix} 1 & 0 & 0 & 0 & 0 & 0 \\ 0 & 1 & 0 & 0 & 0 & 0 \\ 0 & 0 & 1 & 0 & 0 & 0 \end{bmatrix}.$$

where $\hat{v}_{\text{dc}}$ is the peak dc-link voltage, see the appendix.

B. Shoot-Through State

At shoot-through state, the input voltage source and the capacitors charge the inductors, while the diode is cut-off, as shown in Fig. 2(b). During this state, the load is short-circuited since the upper and lower switches in at least one of the three phases are turned on simultaneously, i.e. $u_x = \bar{u}_x = 1$, where $\bar{u}_x$ denotes the position of the lower switch in phase $x \in \{a, b, c\}$. The converter at the shoot-through state is described by the following expression

$$\frac{\mathrm{d}\boldsymbol{x}(t)}{\mathrm{d}t} = \boldsymbol{F}_2\boldsymbol{x}(t) + \boldsymbol{G}_2\boldsymbol{u}_{abc}(t) + \boldsymbol{H}_2\boldsymbol{w}(t) \tag{2a}$$

$$\boldsymbol{y}(t) = \boldsymbol{E}\boldsymbol{x}(t)\,, \tag{2b}$$

where

$$\boldsymbol{F}_2 = \begin{bmatrix} -\frac{R}{L} & 0 & 0 & 0 & 0 & 0 \\ 0 & -\frac{R}{L} & 0 & 0 & 0 & 0 \\ 0 & 0 & 0 & 0 & 0 & \frac{1}{L_1} \\ 0 & 0 & 0 & 0 & \frac{1}{L_2} & 0 \\ 0 & 0 & 0 & -\frac{1}{C_1} & 0 & 0 \\ 0 & 0 & -\frac{1}{C_2} & 0 & 0 & 0 \end{bmatrix},$$

$$\boldsymbol{G}_2 = \hat{v}_{\text{dc}} \begin{bmatrix} \frac{1}{L} & 0 \\ 0 & \frac{1}{L} \\ 0 & 0 \\ 0 & 0 \\ 0 & 0 \\ 0 & 0 \end{bmatrix} \boldsymbol{K}, \qquad \boldsymbol{H}_2 = \begin{bmatrix} 0 \\ 0 \\ \frac{1}{L_1} \\ 0 \\ 0 \\ 0 \end{bmatrix}.$$

C. Continuous-Time Model

Models (1) and (2) can be combined in one model that will describe the boost mode operation of the qZSI. To do so, an auxiliary binary variable d_{aux} is introduced. Variable d_{aux} indicates the state at which the converter operates, i.e.

$$d_{\text{aux}} = \begin{cases} 0 & \text{if non-shoot-through} \\ 1 & \text{if shoot-through} \end{cases}. \tag{3}$$

Since the transition from non-shoot-through state to shoot-through state, and vice versa, is input-dependent, (3) can be written as

$$d_{\text{aux}} = \begin{cases} 0 & \text{if } u_x \neq \bar{u}_x \forall\, x \in \{a, b, c\} \\ 1 & \text{if } \exists\, x \in \{a, b, c\} \text{ s.t. } u_x = \bar{u}_x = 1 \end{cases}. \tag{4}$$

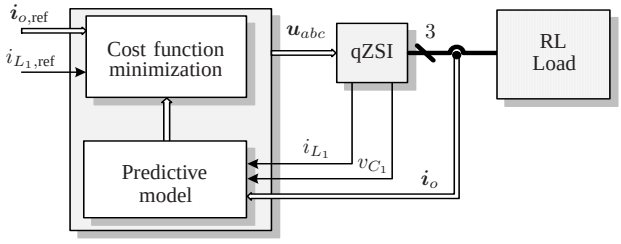

Fig. 3: Direct model predictive control with reference tracking for the qZSI.

Taking the above into account, the model of the converter can be written as

$$\frac{\mathrm{d}\boldsymbol{x}(t)}{\mathrm{d}t} = \boldsymbol{F}\boldsymbol{x}(t) + \boldsymbol{G}\boldsymbol{u}_{abc}(t) + \boldsymbol{H}\boldsymbol{w}(t) \tag{5a}$$

$$\boldsymbol{y}(t) = \boldsymbol{E}\boldsymbol{x}(t)\,, \tag{5b}$$

where

$$\boldsymbol{F} = \begin{bmatrix} -\frac{R}{L} & 0 & 0 & 0 & 0 & 0 \\ 0 & -\frac{R}{L} & 0 & 0 & 0 & 0 \\ 0 & 0 & 0 & 0 & \frac{d_{\text{aux}}-1}{L_1} & \frac{d_{\text{aux}}}{L_1} \\ 0 & 0 & 0 & 0 & \frac{d_{\text{aux}}}{L_2} & \frac{d_{\text{aux}}-1}{L_2} \\ \frac{m_1}{C_1} & \frac{m_2}{C_1} & \frac{1-d_{\text{aux}}}{C_1} & -\frac{d_{\text{aux}}}{C_1} & 0 & 0 \\ \frac{m_1}{C_2} & \frac{m_2}{C_2} & -\frac{d_{\text{aux}}}{C_2} & \frac{1-d_{\text{aux}}}{C_2} & 0 & 0 \end{bmatrix}$$

and

$$m_1 = (d_{\text{aux}}-1)\boldsymbol{u}_{abc}^T\boldsymbol{K}_{(:,1)}^{-1}, \quad m_2 = (d_{\text{aux}}-1)\boldsymbol{u}_{abc}^T\boldsymbol{K}_{(:,2)}^{-1}$$

Moreover,

$$\boldsymbol{G} = \boldsymbol{G}_1 = \boldsymbol{G}_2, \qquad \boldsymbol{H} = \boldsymbol{H}_1 = \boldsymbol{H}_2\,.$$

III. Direct Model Predictive Control With Reference Tracking

The block diagram of the proposed direct predictive controller with current reference tracking is illustrated in Fig. 3. As can be seen, the desirable system performance is achieved by directly manipulating the inverter switches, without the presence of a modulator. The proposed MPC algorithm first computes the evolution of the plant over the prediction horizon (i.e. the trajectories of the variables of concern) based on the measurements of the load and inductor currents and capacitor voltages. Following, the optimal control action (i.e. the switching signals) is chosen by minimizing a performance criterion in real time. Note that according to (9a) $v_{\text{in}} = v_{C_1} - v_{C_2}$, thus it suffices to measure only the input voltage v_{in} and one capacitor voltage v_{C_1}. Moreover, only one inductor current is required to be measured since $i_{L_1} = i_{L_2}$, assuming that $L_1 = L_2$.

A. Internal Control Model

As mentioned above, since $i_{L_1} = i_{L_2}$ only one inductor current is considered as controlled variable. In addition, a direct capacitor voltage control is not necessary since the changes in the capacitor voltage affect the dc side the same way the corresponding changes in the inductor current do. Therefore, only one of the two variables is needed for the control of the dc side in order to boost the dc-link voltage to the desired level.

Considering the above and the model described in Section II, the discrete-time state-space model of the qZSI is of the form

$$\boldsymbol{x}(k+1) = \boldsymbol{A}\boldsymbol{x}(k) + \boldsymbol{B}\boldsymbol{u}_{abc}(k) + \boldsymbol{D}\boldsymbol{w}(k) \tag{6a}$$

$$\boldsymbol{y}(k) = \boldsymbol{C}\boldsymbol{x}(k)\,, \tag{6b}$$

with $\boldsymbol{A} = (\boldsymbol{F}+\boldsymbol{I})T_s$, $\boldsymbol{B} = \boldsymbol{G}T_s$, $\boldsymbol{D} = \boldsymbol{H}T_s$ and $\boldsymbol{C} = \boldsymbol{E}$. Moreover, $\boldsymbol{I}$ denotes the identity matrix, T_s is the sampling interval, and $k \in \mathbb{N}$.

B. Optimal Control Problem

The control objective of the introduced MPC approach for the qZSI is threefold. First, the load current $\boldsymbol{i}_o$ should accurately track its reference value $\boldsymbol{i}_{o,\text{ref}}$. Moreover, the inductor current i_{L_1} should be regulated along its reference trajectory, derived from an outer loop based on a power balance equation. Finally, the switching losses are to be kept small, which is achieved by keeping the switching frequency relatively low.

At time-step k, the cost function that penalizes the error of the output variables and the switching effort over the finite prediction horizon of N time steps is written as

$$J(k) = \sum_{\ell=k}^{k+N-1} ||\boldsymbol{y}_{\text{ref}}(\ell+1|k) - \boldsymbol{y}(\ell+1|k)||_{\boldsymbol{Q}}^2 + ||\Delta\boldsymbol{u}_{abc}(\ell|k)||_{\boldsymbol{R}}^2\,. \tag{7}$$

In (7) $\boldsymbol{y}_{\text{ref}} \in \mathbb{R}^3$ is a vector encompassing the reference values of the output variables, i.e. $\boldsymbol{y}_{\text{ref}} = [i_{o,\alpha,\text{ref}}\ i_{o,\beta,\text{ref}}\ i_{L_1,\text{ref}}]^T$. Moreover, the term $\Delta\boldsymbol{u}_{abc}(k) = \boldsymbol{u}_{abc}(k) - \boldsymbol{u}_{abc}(k-1)$ is added to control the inverter switching frequency by penalizing the switching transitions. Finally, the diagonal, positive semidefinite matrices $\boldsymbol{Q}$ and $\boldsymbol{R} \in \mathbb{R}^{3\times3}$ are the weighting matrices[2] that set the trade-off between the overall tracking accuracy and the switching frequency.

The optimal sequence of control actions is then computed by minimizing (7) over the optimization variable, i.e. the switching sequence over the horizon $\boldsymbol{U}(k) = [\boldsymbol{u}_{abc}^T(k)\ \boldsymbol{u}_{abc}^T(k+1)\ldots\boldsymbol{u}_{abc}^T(k+N-1)]^T$, i.e.

$$\begin{aligned} \underset{\boldsymbol{U}(k)}{\text{minimize}} \quad & J(k) \\ \text{subject to} \quad & \text{eq. (6)} \\ & \boldsymbol{U}(k) \in \mathbb{U}\ . \end{aligned} \tag{8}$$

with $\mathbb{U} = \mathcal{U}^{3N}$. Having found the optimal switching sequence $\boldsymbol{U}^*(k)$, only its first element $\boldsymbol{u}_{abc}^*(k)$ is applied to the qZSI, whereas the rest are discarded. At the next time-step $k+1$, the whole procedure is repeated with updated measurements over a one-step shifted horizon, as the receding horizon policy dictates [10].

[2]The squared norm weighted with the positive (semi)definite matrix $\boldsymbol{W}$ is given by $||\boldsymbol{\xi}||_{\boldsymbol{W}}^2 = \boldsymbol{\xi}^T\boldsymbol{W}\boldsymbol{\xi}$.

C. Reducing the Computational Complexity

As already mentioned, increasing the prediction interval leads to a better system performance. To reduce the consequent increased computational burden, a branch-and-bound algorithm is implemented [18]. Moreover, a depth-first search is performed on the generated search tree, the branches of which are the elements of the candidate solutions of (8), i.e. the elements $\boldsymbol{u}_{abc}(\ell)\,\forall\,\ell = k,\ldots,k+N-1$ of the switching sequences $\boldsymbol{U}(k)$. Hence, the optimal solution is found by exploring each branch of the search tree as far as possible, i.e. until reaching a dead end or the bottom level, where backtracking occurs to explore unvisited nodes in higher layers. Having computed a good upper bound as soon as possible, then suboptimal branches can be pruned at the early stages of the search process, thus reducing the number of the candidate solutions.

To further reduce the computations required, while keeping the prediction horizon long enough, a move blocking technique [19], is utilized in this paper. The main idea of this technique is to split the prediction horizon into two segments, N_1 and N_2, where the total number of prediction steps is $N = N_1+N_2$, with $N_1, N_2 \in \mathbb{N}^+$. The first part of the horizon N_1 is finely sampled with the sampling interval T_s, while the second part N_2 is sampled more coarsely with a multiple of T_s, i.e. with $T_s' = n_s Ts$, where $n_s \in \mathbb{N}^+$. This results in a total prediction interval of $N_1T_s + N_2T_s' = (N_1 + n_sN_2)T_s$, thus, an adequate long prediction horizon is achieved using a few number of prediction steps [20], [21]. Using this technique, and in combination with the aforementioned branch-and-bound strategy, the calculation efforts can be dramatically decreased as shown in Section IV.

IV. Simulation Results

In order to investigate the performance of the proposed MPC scheme for the qZSI, several simulations using MATLAB/Simulink have been conducted. The system parameters are chosen as $v_{\text{in}} = 150\,\text{V}$, $L_1 = L_2 = 1\,\text{mH}$, $C_1 = C_2 = 480\,\mu\text{F}$, $R = 10\,\Omega$, and $L = 10\,\text{mH}$. Based on the desired output power ($P_{\text{out}} = 1.8\,\text{kW}$), the output current reference $\boldsymbol{i}_{o,\text{ref}}$ is set to $10\,\text{A}$, while the inductor current reference is equal to $12\,\text{A}$ ($i_{L_1,\text{ref}} = P_{\text{out}}/v_{\text{in}}$). The sampling interval used is $T_s = 20\,\mu\text{s}$. For the scenarios examined below, the converter operates at a switching frequency of $10\,\text{kHz}$, by setting in (7) $\boldsymbol{Q} = \boldsymbol{I}$ and $\boldsymbol{R} = \lambda_u \boldsymbol{I}$, where $\lambda_u > 0$ is appropriately chosen such that the desired switching frequency results.

First, the steady state operation of both sides of the qZSI is examined at one-step and multi-step prediction horizon. For multi-step horizon, a 4-step horizon ($N = 4$) is chosen, with $N_1 = 3$, $N_2 = 1$, and $n_s = 2$, resulting in a prediction interval of a 5 time steps. Moreover, $\lambda_u = 0.8$ and 1.6 for one-step and 4-step horizon, respectively. The simulation results of the dc-side are illustrated in Figs. 4 and 6 for one and 4-step horizon, respectively. It can be noted that the inductor current tracks its reference (Figs. 4(a) and 6(a)) resulting in a boosted capacitor voltage $v_{C_1} = 200\,\text{V}$ (Figs. 4(b) and 6(b)) and a peak dc-link voltage of $\hat{v}_{\text{dc}} = 250\,\text{V}$ (Figs. 4(c) and 6(c)). The capacitor voltage $v_{C_2} = 50\,\text{V}$ (Figs. 4(b) and 6(b)) is considered as the difference between the capacitor voltage v_{C_1} and the input voltage v_{in}, which is in line with (9a). Moreover, the peak dc-link voltage ($250\,\text{V}$) is the sum of both capacitors voltages ($200\,\text{V} + 50\,\text{V}$), which corresponds to (10). Although both cases (one and 4-step horizon) exhibit good steady-state behavior, the 4-step horizon introduces less ripples and a better overall performance at the same switching frequency. The ac-side results are shown in Figs. 5 and 7 for one and 4-step horizon, respectively. As can be seen in Figs. 5(a) and 7(a), where the three-phase output currents are depicted along with their references, the tracking accuracy of the proposed controller is not affected by the shoot-through state. Moreover, at the same switching frequency ($10\,\text{kHz}$), MPC with a 4-step horizon achieves a current total harmonic distortion (THD) of 2.60% (see Fig. 7(b)), significantly lower than that with the one-step horizon, which is 6.76% (see Fig. 5(b)).

Table I summarizes the computational burden of the proposed MPC algorithm, by showing the number of the complete switching sequences $\boldsymbol{U}$ that are evaluated at each time-step to obtain the optimal solution. More specifically, the average and the maximum number of examined sequences ϕ are displayed for different lengths of the prediction horizon. To highlight the computational efficiency of the proposed MPC algorithm, the number of the switching sequences evaluated with the exhaustive enumeration algorithm—typically used in the field of power electronics to solve MPC problems of the form (8) [11]—is also shown. As can be seen, thanks to the branch-and-bound strategy and the move blocking scheme, the number of examined sequences is significantly reduced. For example, for a prediction interval of 5 time steps—corresponding to a 5-step horizon with exhaustive enumeration, and a 4-step horizon with the move blocking—the maximum number of sequences—which is of importance for a real-time implementation since it corresponds to the worst-case scenario—is reduced by about 97%. Finally, the resulting output current THD is illustrated to emphasize that when longer prediction intervals are implemented the closed-loop system performance can be improved.

Moreover, the transient response of the proposed MPC strategy for the qZSI is examined with a 4-step horizon and switching frequency of $10\,\text{kHz}$. The output current is stepped up from $7\,\text{A}$ to $10\,\text{A}$. Accordingly, the inductor current reference changes from $6\,\text{A}$ to $12\,\text{A}$. The dc- and ac-side results are shown in Figs. 8 and 9, respectively. As for the dc-side, the inductor current accurately tracks its reference (Fig. 8(a)), consequently the capacitor voltage v_{C_1} is changed from $180\,\text{V}$ to $200\,\text{V}$ (Fig. 8(b)). This change results in a change in the peak dc-link voltage $\hat{v}_{\text{dc}}$ from $200\,\text{V}$ to $250\,\text{V}$ (Fig. 8(c)). As can be seen in Fig. 9, the output current is quickly and effectively tracked.

V. Conclusion

This paper proposes a direct model predictive current control scheme with reduced computational complexity for the

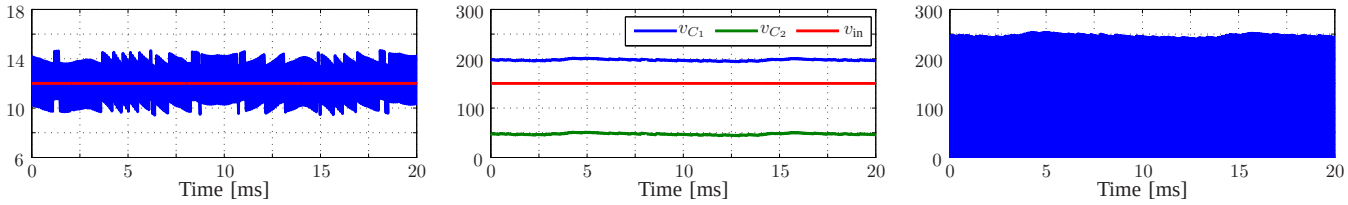

(a) Inductor current i_{L_1} and its reference in [A] (b) Input v_{in} and capacitor voltages v_{C_1}, v_{C_2} in [V] (c) Dc-link voltage v_{dc} in [V]

Fig. 4: Simulation results of the dc-side of the qZSI with one-step horizon. The sampling interval is $T_s = 20\,\mu$s and $\lambda_u = 0.8$. The switching frequency is approximately 10 kHz.

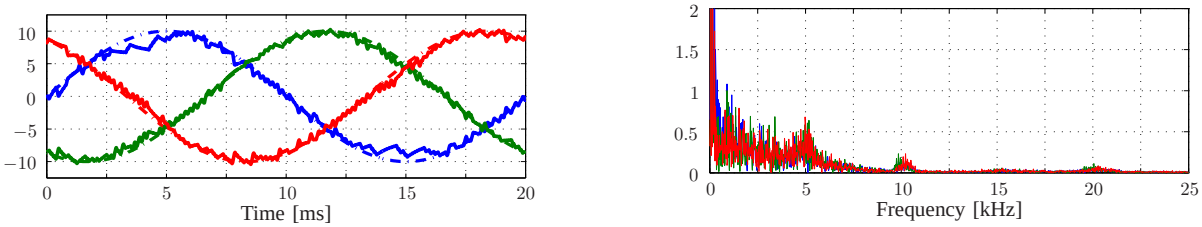

(a) Three-phase output current $\boldsymbol{i}_{\text{o,abc}}$ (solid lines) and their references (dash-dotted lines) in [A]

(b) Output current spectrum (%)

Fig. 5: Simulation results of the ac-side of the qZSI with one-step horizon. The sampling interval is $T_s = 20\,\mu$s and $\lambda_u = 0.8$. The switching frequency is approximately 10 kHz and the output current THD 6.76%.

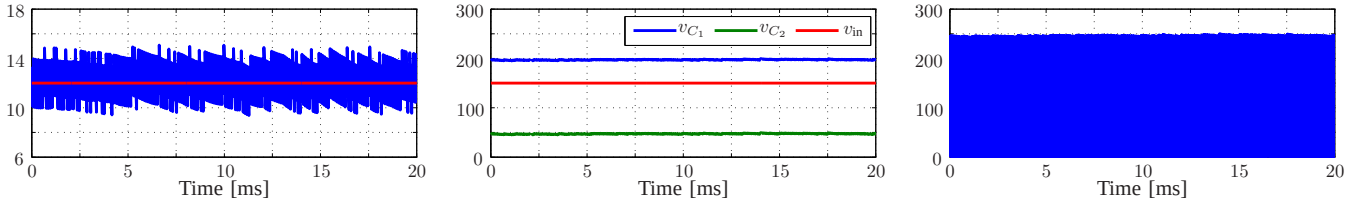

(a) Inductor current i_{L_1} and its reference in [A] (b) Input v_{in} and capacitor voltages v_{C_1}, v_{C_2} in [V] (c) Dc-link voltage v_{dc} in [V]

Fig. 6: Simulation results of the dc-side of the qZSI with a 4-step horizon ($N = 4$—$N_1 = 3$, $N_2 = 1$, $n_s = 2$). The resulting prediction interval is 5 time steps. The sampling interval is $T_s = 20\,\mu$s and $\lambda_u = 1.6$. The switching frequency is approximately 10 kHz.

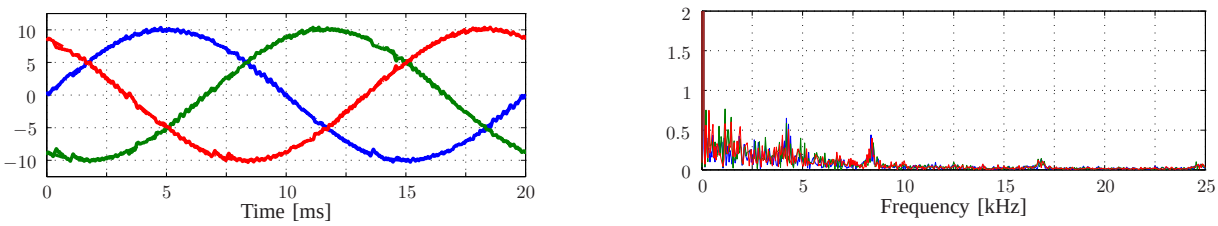

(a) Three-phase output current $\boldsymbol{i}_{\text{o,abc}}$ (solid lines) and their references (dash-dotted lines) in [A]

(b) Output current spectrum (%)

Fig. 7: Simulation results of the ac-side of the qZSI with a 4-step horizon ($N = 4$—$N_1 = 3$, $N_2 = 1$, $n_s = 2$). The resulting prediction interval is 5 time steps. The sampling interval is $T_s = 20\,\mu$s and $\lambda_u = 1.6$. The switching frequency is approximately 10 kHz and the output current THD 2.60%.

TABLE I: The average and the maximum numbers of the examined switching sequences ϕ depending on the length of the prediction horizon (with $n_s = 2$). The resulting output current THD for each case is also shown.

Length of Prediction	Exhaustive Search		Proposed MPC Strategy			
Horizon $NT_s = (N_1 + n_s N_2)T_s$	$N_1 + N_2$	ϕ	$N_1 + N_2$	avg(ϕ)	max(ϕ)	THD %
1	$1+0$	8	$1+0$	8	8	6.76
2	$2+0$	64	$2+0$	53	64	3.97
3	$3+0$	512	$1+1$	54	64	3.31
4	$4+0$	4,096	$2+1$	179	400	2.96
5	$5+0$	32,256	$3+1$	460	1,048	2.60
6	$6+0$	262,144	$2+2$	546	1,344	2.42
7	$7+0$	2,097,152	$3+2$	1,146	3,384	2.10
8	$8+0$	16,777,216	$2+3$	2,699	11,088	1.90

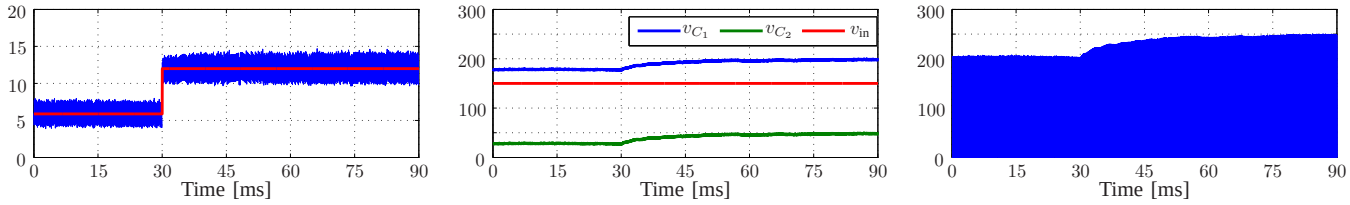

(a) Inductor current i_{L_1} and its reference in [A] (b) Input v_{in} and capacitor voltages v_{C_1}, v_{C_2} in [V] (c) Dc-link voltage v_{dc} in [V]

Fig. 8: Simulation results of the dc-side of the qZSI under a step change in the output current with a 4-step horizon ($5T_s$ prediction horizon length). The sampling interval is $T_s = 20\,\mu$s and $\lambda_u = 1.6$. The switching frequency is approximately 10 kHz.

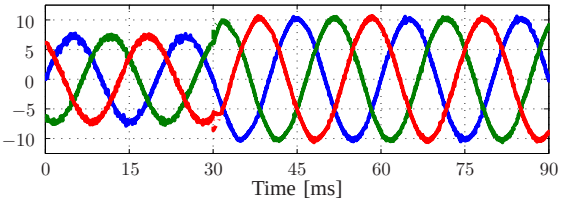

Fig. 9: Simulation results of the ac-side of the qZSI under a step change in the output current with a 4-step horizon ($5T_s$ prediction horizon length). The sampling interval is $T_s = 20\,\mu$s and $\lambda_u = 1.6$. The switching frequency is approximately 10 kHz.

quasi-Z-source inverter. A significant improvement in the system performance can be achieved, as quantified by the output current THD, when using long prediction horizons. However, when considering long prediction horizons, enumeration of all candidate solutions becomes computationally prohibitive. To solve the underlying optimization problem in real time, a nontrivial prediction horizon—as resulted from a move blocking scheme—is implemented which, combined with a branch-and-bound technique, allows to keep the computational burden modest.

APPENDIX

At steady-state operation and according to the inductor volt-second balance, the average voltage of the inductors should be zero. Therefore, the voltages of the capacitors C_1 and C_2, v_{C_1} and v_{C_2}, respectively, as well as the currents i_{L_1} and i_{L_2} of the inductors L_1 and L_2, respectively, are deduced as follows:

$$v_{C_1} = \frac{1-d}{1-2d} v_{\text{in}}\,, \quad v_{C_2} = \frac{d}{1-2d} v_{\text{in}} \tag{9a}$$

$$i_{L_1} = i_{L_2} = \frac{1-d}{1-2d} i_{\text{load}}\,, \tag{9b}$$

where d is the shoot-through duty cycle of the qZSI, and i_{load} the load current as shown in Fig. 2(a). The peak value of the dc-link voltage during the non-shoot-through period is

$$\hat{v}_{\text{dc}} = v_{C_1} + v_{C_2} = \frac{1}{1-2d} v_{\text{in}} = b v_{\text{in}} \tag{10}$$

where $b \geq 1$ is the boost factor resulting from the shoot-through period.

REFERENCES

[1] F. Z. Peng, "Z-source inverter," *IEEE Trans. Ind. Appl.*, vol. 39, no. 2, pp. 504–510, 2003.

[2] A. Ayad, S. Hanafiah, and R. Kennel, "A comparison of quasi-Z-source inverter and traditional two-stage inverter for photovoltaic application," in *Proc. Int. Expo. and Conf. Power Electron., Intelligent Motion, Renew. Energy Management*, Nuremberg , Germany, May 2015, pp. 1–8.

[3] J. Anderson and F. Peng, "Four quasi-Z-source inverters," in *Proc. IEEE Power Electron. Spec. Conf.*, Rhodes, Greece, Jun. 2008, pp. 2743–2749.

[4] Y. Li, S. Jiang, J. Cintron-Rivera, and F. Z. Peng, "Modeling and control of quasi-Z-source inverter for distributed generation applications," *IEEE Trans. Ind. Electron.*, vol. 6039, no. 4, pp. 1532–1541, Apr. 2013.

[5] O. Husev, C. Roncero-Clemente, S. Stepenko, D. Vinnikov, and E. Romero-Cadaval, "CCM operation analysis of the single-phase three-level quasi-Z-source inverter," in *Proc. Int. Power Electron. and Motion Control Conf. and Expo.*, Novi Sad, Serbia, Sep. 2012, pp. DS1b.21–1–DS1b.21–6.

[6] C. J. Gajanayake, D. M. Vilathgamuwa, and P. C. Loh, "Development of a comprehensive model and a multiloop controller for Z-source inverter DO systems," *IEEE Trans. Ind. Electron.*, vol. 54, pp. 2352–2359, Aug. 2007.

[7] J. Liu, S. Jiang, D. Cao, and F. Z. Peng, "A digital current control of quasi-Z-source inverter with battery," *IEEE Trans. Ind. Informat.*, vol. 9, no. 2, pp. 928–937, May 2013.

[8] A. H. Rajaei, S. Kaboli, and A. Emadi, "Sliding mode control of Z-source inverter," in *Proc. IEEE Ind. Electron. Conf.*, Nov. 2008, pp. 947–952.

[9] H. Rostami and D. A. Khaburi, "Neural networks controlling for both the dc boost and ac output voltage of Z-source inverter," in *Proc. Power Electron. Drive System Technology Conf.*, Feb. 2010, pp. 135–140.

[10] J. B. Rawlings and D. Q. Mayne, *Model Predictive Control: Theory and Design*. Madison, WI: Nob Hill, 2009.

[11] P. Cortés, M. P. Kazmierkowski, R. M. Kennel, D. E. Quevedo, and J. Rodríguez, "Predictive control in power electronics and drives," *IEEE Trans. Ind. Electron.*, vol. 55, no. 12, pp. 4312–4324, Dec. 2008.

[12] T. Geyer, "Low complexity model predictive control in power electronics and power systems," Ph.D. dissertation, Autom. Control Lab. ETH Zurich, Zurich, Switzerland, 2005.

[13] P. Karamanakos, "Model predictive control strategies for power electronics converters and ac drives," Ph.D. dissertation, Elect. Mach. and Power Electron. Lab. NTU Athens, Athens, Greece, 2013.

[14] W. Mo, P. Loh, and F. Blaabjerg, "Model predictive control for Z-source power converter," in *Proc. IEEE Int. Conf. Power Electron. and ECCE Asia*, May/Jun. 2011, pp. 3022–3028.

[15] A. Ayad and R. Kennel, "Model predictive controller for grid-connected photovoltaic based on quasi-Z-source inverter," in *Proc. IEEE Int. Symp. Pred. Control of Elect. Drives and Power Electron.*, Munich, Germany, Oct. 2013, pp. 1–6.

[16] ——, "Direct model predictive control of quasi-Z-source inverter compared with the traditional PI-based PWM control," in *Proc. Eur. Power Electron. Conf.*, Geneva, Switzerland, Sep. 2015, to appear.

[17] T. Geyer, P. Karamanakos, and R. Kennel, "On the benefit of long-horizon direct model predictive control for drives with LC filters," in *Proc. IEEE Energy Convers. Congr. Expo.*, Pittsburgh, PA, Sep. 2014, pp. 3520–3527.

[18] E. L. Lawler and D. E. Wood, "Branch-and-bound methods: A survey," *Op. Res.*, vol. 14, no. 4, pp. 699–719, Jul./Aug. 1966.

[19] R. Cagienard, P. Grieder, E. C. Kerrigan, and M. Morari, "Move blocking strategies in receding horizon control," *J. of Process Control*, vol. 17, no. 6, pp. 563–570, Jul. 2007.

[20] P. Karamanakos, T. Geyer, and S. Manias, "Direct voltage control of dc-dc boost converters using enumeration-based model predictive control," *IEEE Trans. Power Electron.*, vol. 29, no. 2, pp. 968–978, Feb. 2014.

[21] P. Karamanakos, T. Geyer, N. Oikonomou, F. D. Kieferndorf, and S. Manias, "Direct model predictive control: A review of strategies that achieve long prediction intervals for power electronics," *IEEE Ind. Electron. Mag.*, vol. 8, no. 1, pp. 32–43, Mar. 2014.